More wavelet-like orthonormal bases for the lowest Landau level: some considerations

1994 J. Phys. A: Math. Gen. 27 5583

(http://iopscience.iop.org/0305-4470/27/16/023)

J. Phys. A: Math. Gen. 27 (1994) 5583–5597. Printed in the UK

More wavelet-like orthonormal bases for the lowest Landau level: some considerations

F Bagarello†

Dipartimento di Matematica ed Applicazioni, Facoltá di Ingegneria, Universitá di Palermo, I-90128 Palermo, Italy

Received 11 February 1994, in final form 29 April 1994

Abstract. In a previous work, J P Antoine and I have discussed a general procedure which 'projects' arbitrary orthonormal bases of $L^2(\mathbb{R})$ into orthonormal bases of the lowest Landau level. In this paper, we apply this procedure to a certain number of examples, with particular attention to the spline bases. We also discuss Haar, Littlewood–Paley and Journé bases.

1. Introduction

In a previous paper [1], Antoine and the author have discussed in some detail how wavelet theory and multi-resolution analysis (MRA) can be used in the description of two-dimensional electron systems, with particular attention to the fractional quantum Hall effect (FQHE).

The first step in discussing this effect consists of finding a good description of the ground state of the finite-volume (V) system (with a finite number (N) of electrons) and then to consider its thermodynamical limit (V and $N \to \infty$). In [2] the authors have shown that, for a certain range of electron density, the correlations between the electrons do not significantly lower the energy of the system and, in fact, a Slater determinant of single-electron wavefunctions (with Gaussian behaviour in x and y) is a good candidate for the ground state of the Hamiltonian. Out of this range, however, the Laughlin wavefunction [3] is energetically favoured [2] so that a phase transition is expected for a certain 'critical' electron density. The experiments follow this same direction [4] but the experimental and theoretical values of these 'critical' densities differ slightly so that an improvement of the theoretical results is needed. Moreover, the hierarchical structure discussed in [5] and in other works cannot easily be recovered using the wavefunction proposed in [2] or other wavefunctions of the same kind. This hierarchical structure is, on the contrary, naturally present in wavelet theory so that it is natural to ask whether this framework could help in understanding the intrinsic nature of the FQHE. Another reason suggesting the use of wavelets is the necessity of minimizing the trial ground-state energy. We know, in fact, that a better localization of the single-electron wavefunction is reflected into a lower energy of the corresponding Slater determinant [2]. Therefore, the existence of a natural parameter which controls the support of the constructed functions starting from a given mother wavelet might be conveniently used in the description of the FQHE.

With these considerations in mind, it is clear why we prefer to construct new 'wavelet' bases instead of using already existing bases such as the ones proposed in [2, 3, 6].

† E-mail: Bagarello@ipamat.math.unipa.it

0305-4470/94/165583+15$19.50

The Hamiltonian of a single electron constrained in a plane and subjected to a strong magnetic field orthogonal to the plane is

$$H_0 = \tfrac{1}{2}(Q'^2 + P'^2) \tag{1.1}$$

where $Q' = p_y + x/2$ and $P' = p_x - y/2$.

In [1] it is shown that any single-electron basis $\{\Psi_n(x, y) : n \in \mathbb{Z}\}$ for the lowest Landau level (LLL) can be conveniently expressed by

$$\Psi_n(x, y) = \frac{e^{ixy/2}}{\sqrt{2}\pi^{3/4}} \int_{-\infty}^{\infty} e^{iyP} e^{-(x+P)^2/2} h_n(P)\, dP \tag{1.2}$$

where the set $\{h_n(P)\}$ is the corresponding basis in $L^2(\mathbb{R})$. Moreover, if $\langle h_n, h_m \rangle = \delta_{nm}$, it is also easy to prove that the functions of the set $\{\Psi_n(x, y) : n \in \mathbb{Z}\}$ are mutually orthogonal.

Formula (1.2) has a certain utility for discussing the asymptotic behaviour of the function $\Psi_n(x, y)$ in x: it is easy to see, in fact, that the asymptotic behaviour of $\Psi_n(x, y)$ for large $|x|$ is governed by the asymptotic behaviour of $h_n(P)$. One can also show that the behaviour in y, for $|y| \gg 1$, is related to the behaviour of $\tilde{h}_n(Q)$ for $|Q| \gg 1$, the Fourier transform of $h_n(P)$. We will come back to this point in the next section. The possibility of controlling the asymptotic behaviour of $\Psi_n(x, y)$ is crucial since we have in mind to add a Coulomb interaction between the electrons. Such an addition causes an increment in the energy of the system which is minimized if the single-electron wavefunctions are localized as much as possible and their relative orthogonality kept untouched. This is the reason why the Wigner crystal, in which the electrons are extremely localized (they are actually described by delta functions), gives a lower bound for the energy of the two-dimensional electron gas. As we have already mentioned, wavelets seem to be the natural choice for the best control of this localization property. We know, in fact, that if $h(x)$ is an opportune mother wavelet [7] then the set $\{h_{mn}(x), m, n \in \mathbb{Z}\} \equiv \{2^{-m/2} h(2^{-m}x - n), m, n \in \mathbb{Z}\}$ is formed by mutually orthonormal functions whose support is controlled by the value of the scale parameter m.

In [1] the authors have discussed in some detail two examples of wavelet-like bases for the LLL, both coming from MRA: the Haar and the Littlewood–Paley bases. They have been selected from all the known examples of orthonormal bases in $L^2(\mathbb{R})$ constructed using wavelet theory because they are the only known examples coming from MRA for which the integral in (1.2) can be computed analytically. In the following, we give more information about the above examples and we explore the projections of the Journé basis and some cardinal splines in the LLL.

The paper is organized as follows. In the next section, we give some useful information related to formula (1.2). In section 3, we return to the Haar and the Littlewood–Paley bases, adding some considerations to the bases already discussed in [1]. In section 4, we study, in some detail, the Journé basis. We end the paper with a section devoted to cardinal splines.

2. General considerations

In this section, we give some information and results concerning formula (1.2) which will be used in the rest of the paper.

As already seen in [1], it may be convenient to use the Fourier transform of the mother wavelet for computing the set $\{\Psi_n(x, y)\}$ spanning the LLL. The Littlewood–Paley basis, for instance, is originated by the mother wavelet

$$\Phi(P) \equiv (\pi P)^{-1}(\sin(2\pi P) - \sin(\pi P)) \tag{2.1}$$

which, when used to compute the integral in (1.2), with the identification

$$h_n(P) \to \Phi_{mn}(P) \equiv 2^{-m/2}\Phi(2^{-m}P - n)$$

makes the integration very difficult. Nevertheless, recalling that

$$\Phi_{mn}(P) = \frac{2^{-m/2}}{\sqrt{2\pi}} \int_{-\infty}^{\infty} \tilde{\Phi}(\omega) e^{i\omega(2^{-m}P - n)}\, d\omega$$

we can use the following form for $\tilde{\Phi}(\omega)$ [7]:

$$\tilde{\Phi}(\omega) = \begin{cases} (2\pi)^{-1/2} & \text{if } \pi \leqslant |\omega| \leqslant 2\pi \\ 0 & \text{otherwise} \end{cases} \tag{2.2}$$

and try to exchange the order of integration in formula (1.2) using the Fubini theorem. This exchange was discussed in [1] for the $\tilde{\Phi}(\omega)$ above and claimed to be possible. We can generalize this result to a large class of functions $\tilde{\Phi}(\omega)$ from the following proposition whose proof is omitted due to its simplicity.

Proposition. For any $\tilde{\Phi}(\omega) \in L^1(\mathbb{R})$, we have

$$\begin{aligned} \Psi_{mn}(x, y) &\equiv \frac{e^{ixy/2} 2^{-m/2}}{\sqrt{2}\pi^{3/4}} \int_{-\infty}^{\infty} e^{iyP} e^{-(x+P)^2/2} \Phi(2^{-m}P - n)\, dP \\ &= \frac{e^{-ixy/2} 2^{-m/2}}{\sqrt{2}\pi^{3/4}} \int_{-\infty}^{\infty} \tilde{\Phi}(\omega) e^{-i\omega(n + x2^{-m})} e^{-(y + 2^{-m}\omega)^2/2}\, d\omega. \end{aligned} \tag{2.3}$$

Remarks.

(i) In the proof of the above proposition, a crucial role is played by the presence of the Gaussian $e^{-(x+P)^2/2}$ in (1.2), which ensures the fast convergence of the integral.

(ii) The function $\tilde{\Phi}(\omega)$ in (2.2) belongs to $L^1(\mathbb{R})$. Therefore, the order of integration can be interchanged, according to the claims made in [1].

This exchange of integrals will also be possible for the Journé and spline bases.

We now discuss, in more detail, the link between the asymptotic behaviours of $\Psi_{00}(x, y)$, $\Phi(P)$ and $\tilde{\Phi}(\omega)$. The behaviour of $\Psi_{mn}(x, y)$ can be analysed in the same way with analogous conclusions. We give here mainly heuristic arguments, which, however, are sufficient to suggest the way in which things go. The same results can be found rigorously.

From the first part of formula (2.3) it is evident that, if $|x|$ is very large, the integral can be restricted to a small neighbourhood of $-x$ because the integrand is significantly different from zero only in this region. We therefore expect that, neglecting the overall phase and an irrelevant constant,

$$\lim_{|x|\to\infty} \Psi_{00}(x, y_0) \simeq \lim_{|x|\to\infty} \Phi(-x)$$

where y_0 is fixed.

In order to study the behaviour of $\Psi_{00}(x, y)$ in y, it is convenient to use the right-hand side of equation (2.3). The reason is clear: in this equation, the variable which enters in the Gaussian is y, so the same argument as before can be repeated. In particular, the main contribution to the integral in (2.3) comes for $\omega \simeq -y$, if $|y|$ is very large. Therefore, again forgetting irrelevant constants and phases, we find

$$\lim_{|y|\to\infty} \Psi_{00}(x_0, y) \simeq \lim_{|y|\to\infty} \tilde{\Phi}(-y)$$

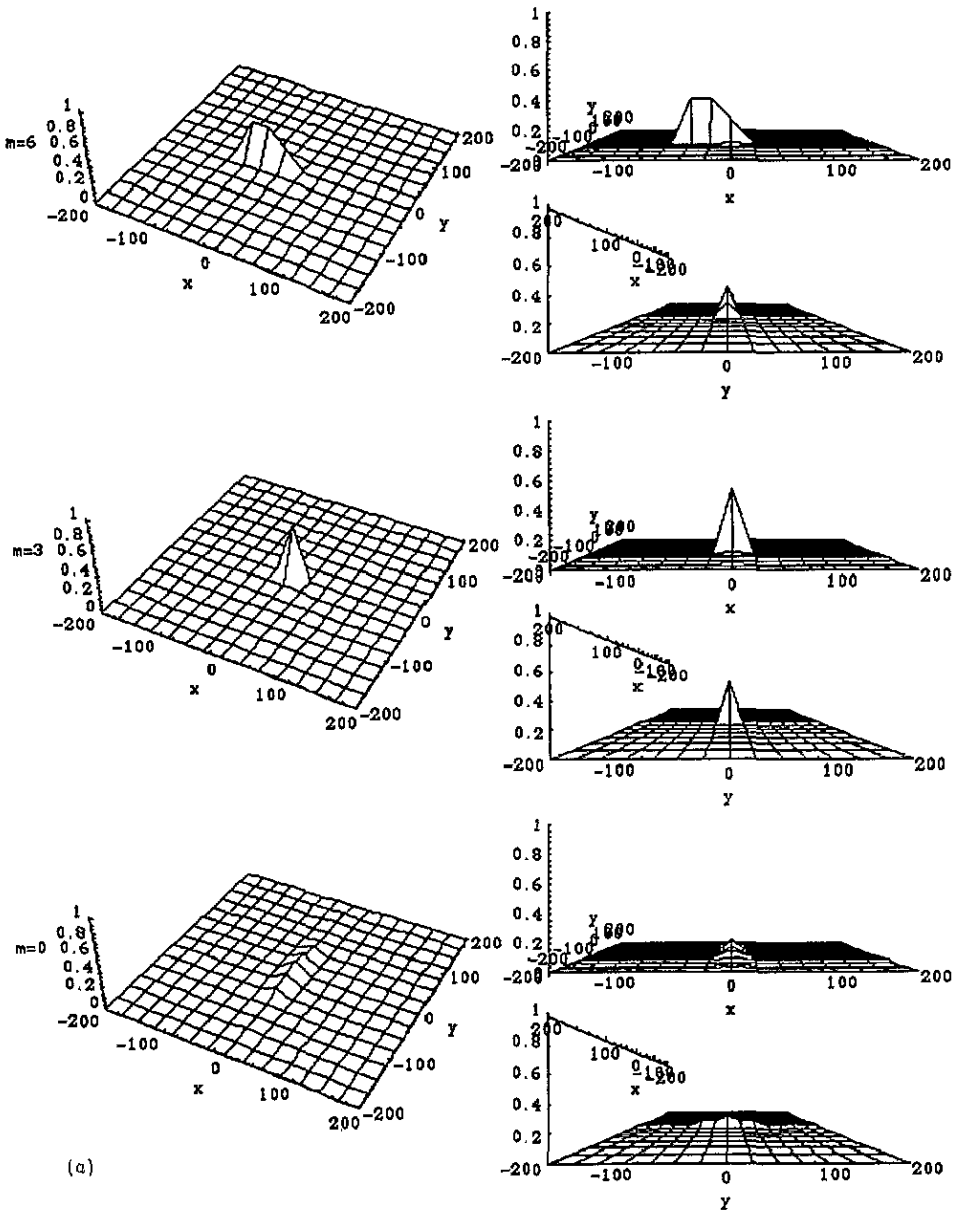

Figure 1. $|H_{m0}(x, y)|$ with (*a*) $m = 6, 3, 0$ and $x, y \in [-200, 200]$; (*b*) $m = -3, -6$ and $x, y \in [-200, 200]$.

where x_0 is fixed.

In conclusion, we deduce that, if $\Phi(x)$ has compact support (so that $\tilde{\Phi}(\omega)$ is delocalized), the decay of $\Psi_{00}(x, y)$ is very fast in x but rather slow in y. The opposite situation is expected if $\tilde{\Phi}(\omega)$ has compact support.

The rigorous statement, which was communicated to the author by Dr G Morchio, is as follows. If α is any real number such that $\lim_{|P|\to\infty} P^{\alpha}\Phi(P) < \infty$ then it also follows

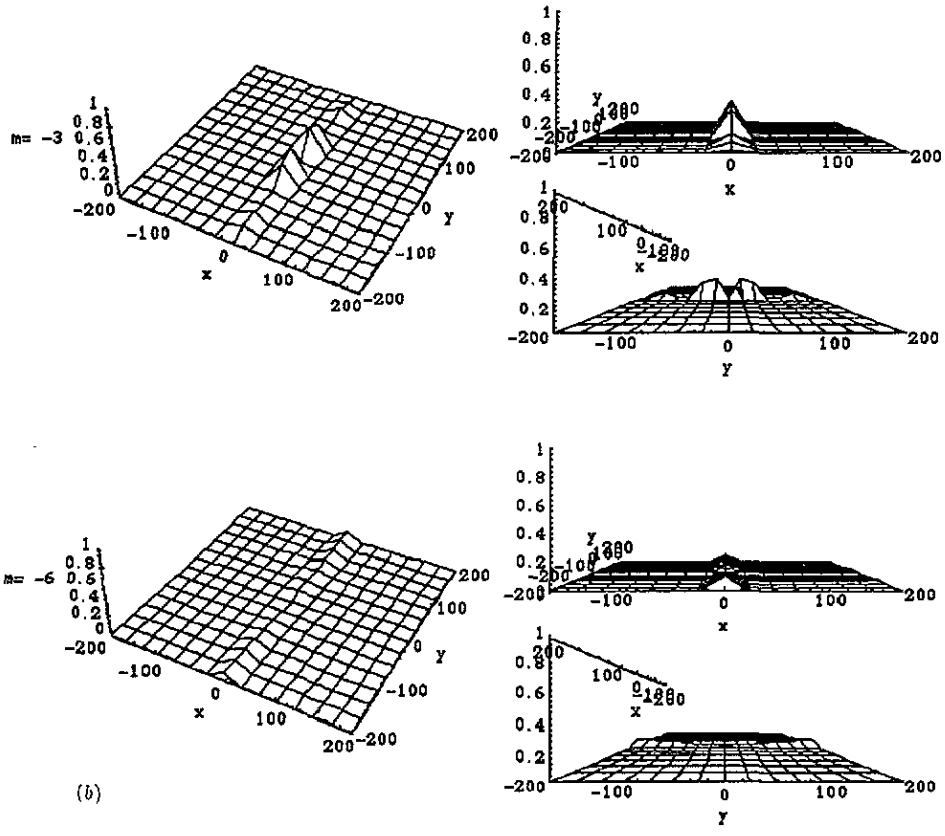

Figure 1. (Continued)

that $\lim_{|x|\to\infty} x^{\alpha}\Psi_{00}(x, y_0) < \infty$.

An analogous statement holds for the decay of $\Psi_{00}(x, y)$ in y.

3. The Haar and Littlewood–Paley bases

In [1] Antoine and the author have found the explicit form of the projections of the Haar and Littlewood–Paley bases in the LLL, obtained using formula (2.3).

The Haar basis is constructed by starting with the function

$$h(x) = \begin{cases} 1 & \text{if } 0 \leqslant x < \frac{1}{2} \\ -1 & \text{if } \frac{1}{2} \leqslant x < 1 \\ 0 & \text{otherwise} \end{cases} \tag{3.1}$$

whose Fourier transform $\tilde{h}^{(H)}(\omega) = 1/\sqrt{2\pi}\int_{-\infty}^{\infty} h(x)e^{-i\omega x}\,dx$ is $\tilde{h}^{(H)}(\omega) = (1 - e^{-i\omega/2})^2/i\omega\sqrt{2\pi}$. As expected, we see that $\tilde{h}^{(H)}(\omega)$ decays like $1/\omega$.

In [1] it is proved that the projections in the LLL of the Haar orthonormal functions $h_{mn}(x) = 2^{-m/2}h(2^{-m}x - n)$ are

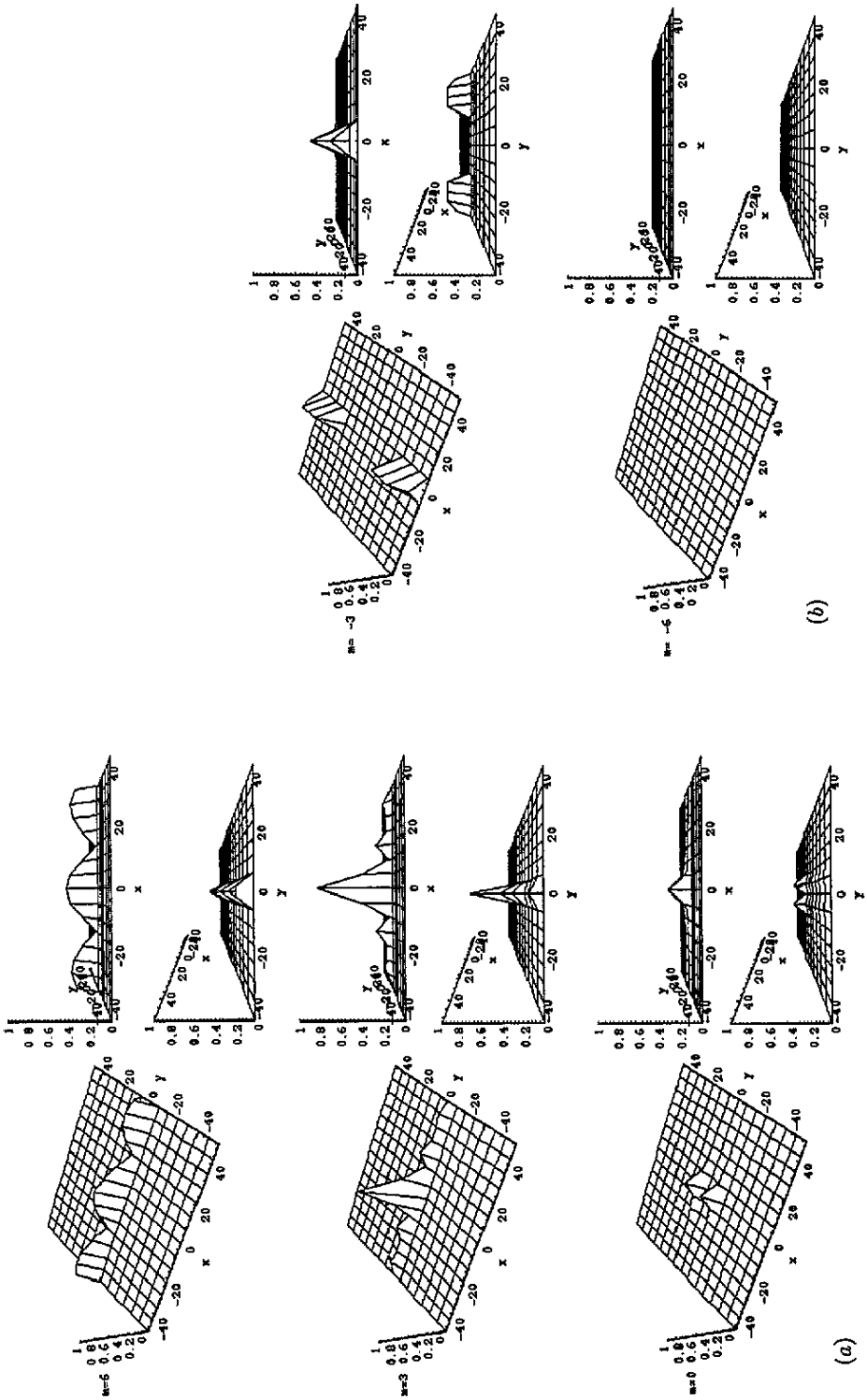

Figure 2. $|\Psi_{m0}^{(LP)}(x,y)|$ with (*a*) $m = 6, 3, 0$ and $x, y \in [-50, 50]$; (*b*) $m = -3, -6$ and $x, y \in [-50, 50]$; (*c*) $m = 6, 3, 0$ and $x, y \in [-200, 200]$; (*d*) $m = -3, -6$ and $x, y \in [-200, 200]$.

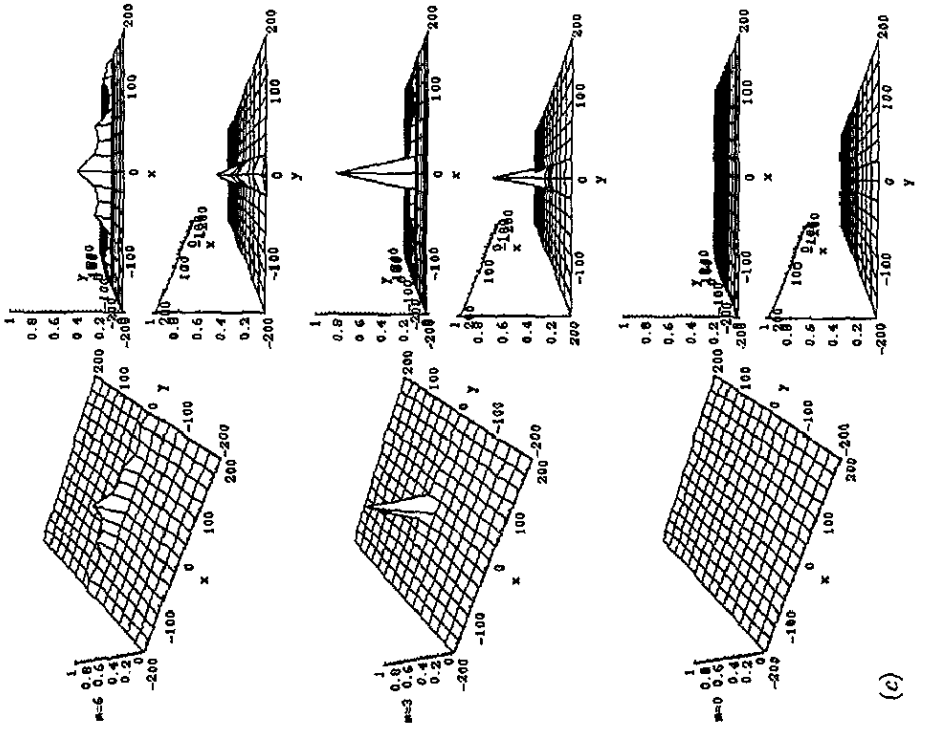

Figure 2. (Continued)

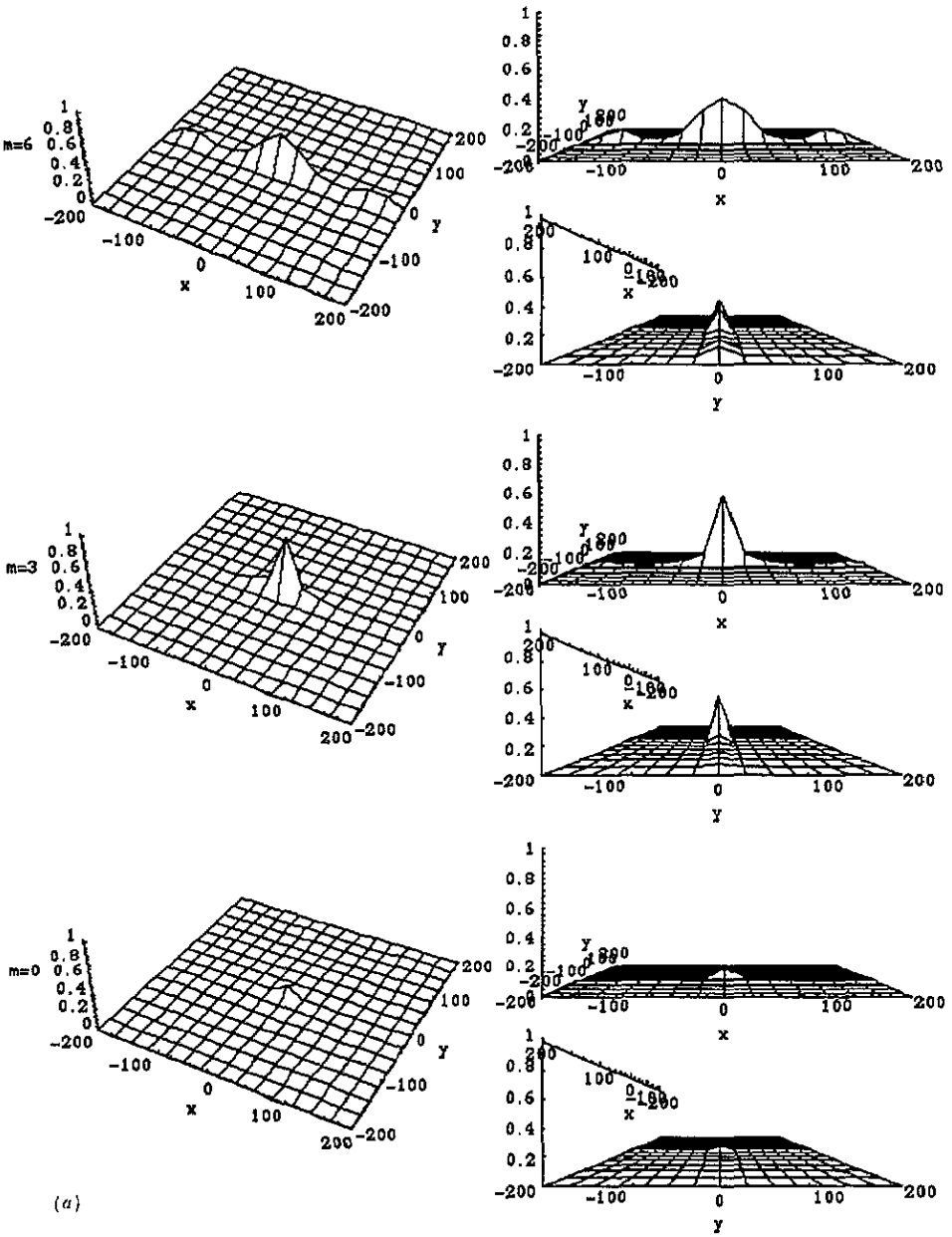

(a)

Figure 3. $|\Psi^{(J)}_{m0}(x, y)|$ with (*a*) $m = 6, 3, 0$ and $x, y \in [-200, 200]$, (*b*) $m = -3, -6$ and $x, y \in [-200, 200]$.

$$H_{mn}(x, y) = \frac{e^{-ixy/2}e^{-y^2/2}}{2\pi^{1/4}}2^{-m/2}\left\{2\Phi\left(\frac{x - iy + 2^m n + 2^{m-1}}{\sqrt{2}}\right) - \Phi\left(\frac{x - iy + 2^m n}{\sqrt{2}}\right)\right.$$
$$\left. - \Phi\left(\frac{x - iy + 2^m n + 2^m}{\sqrt{2}}\right)\right\}. \tag{3.2}$$

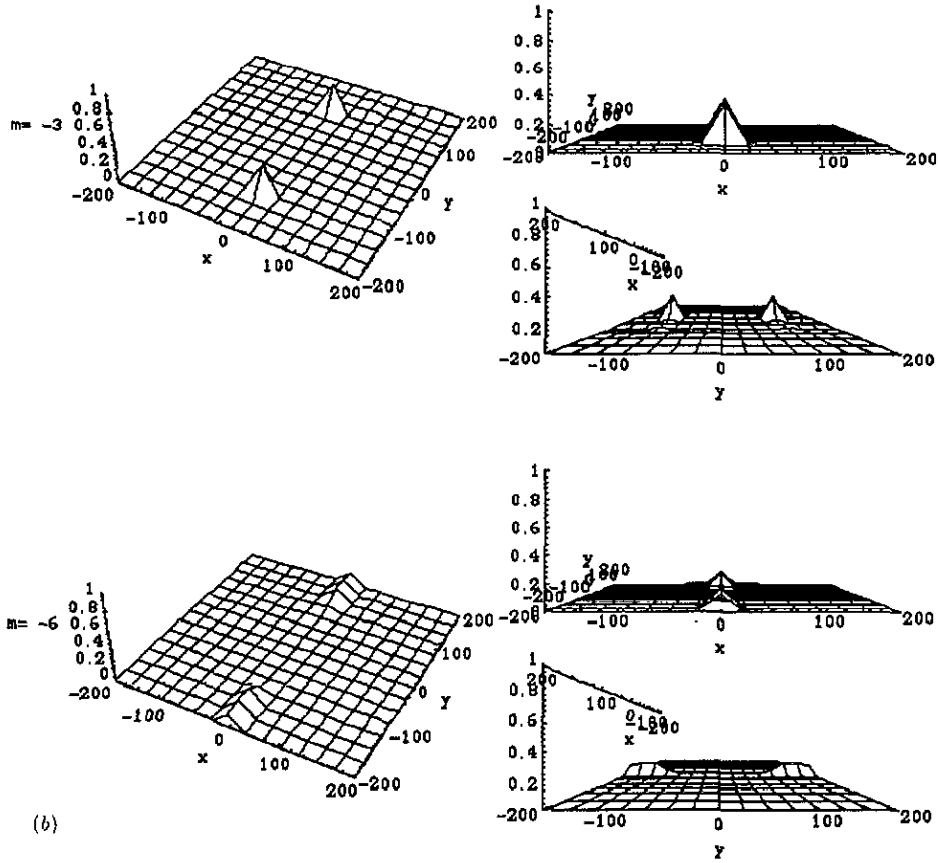

Figure 3. (Continued)

Here, the probability function $\Phi(x)$ is defined by the integral

$$\Phi(x) \equiv \frac{2}{\sqrt{\pi}} \int_0^x \mathrm{e}^{-t^2}\,\mathrm{d}t$$

(see [8]).

In [1] we have plotted the modulus of $H_{00}(x, y)$ and the asymptotic behaviour in x and y has been discussed: as we expect from the general discussion of the previous section, we have seen that the decay in x is very fast, actually exponential, while $|H_{00}(x, y)|$ behaves like $1/y$ in y. This is obviously linked to the fact that $h(x)$ has compact support while $\tilde{h}^{(\mathrm{H})}(\omega)$ decays like $1/\omega$.

Figure 1 shows an analogous behaviour even for $m \neq 0$. Here, and in the following, we always fix $n = 0$ since the value of n does not affect the supports of the wavefunction.

Recalling the definition of the set $\{h_{mn}(x)\}$, we see that, for increasing m ($m = 1, 2, 3, \ldots$), the support of $h_{mn}(x)$ increases as well so that the decay in x of the related function in the LLL is expected to be slower. On the other hand, if m decreases ($m = -1, -2, -3, \ldots$), then the support of $h_{mn}(x)$ shrinks and, therefore, $H_{mn}(x, y)$ goes to zero faster in x. Even if we do not expect a direct influence of the value of m on the asymptotic behaviour of $H_{mn}(x, y)$ in y, due to the reasons discussed in the previous section, a minor influence is nevertheless unavoidable. This follows essentially from the normalization requirement of the wavefunctions. In fact, if the maxima of the different

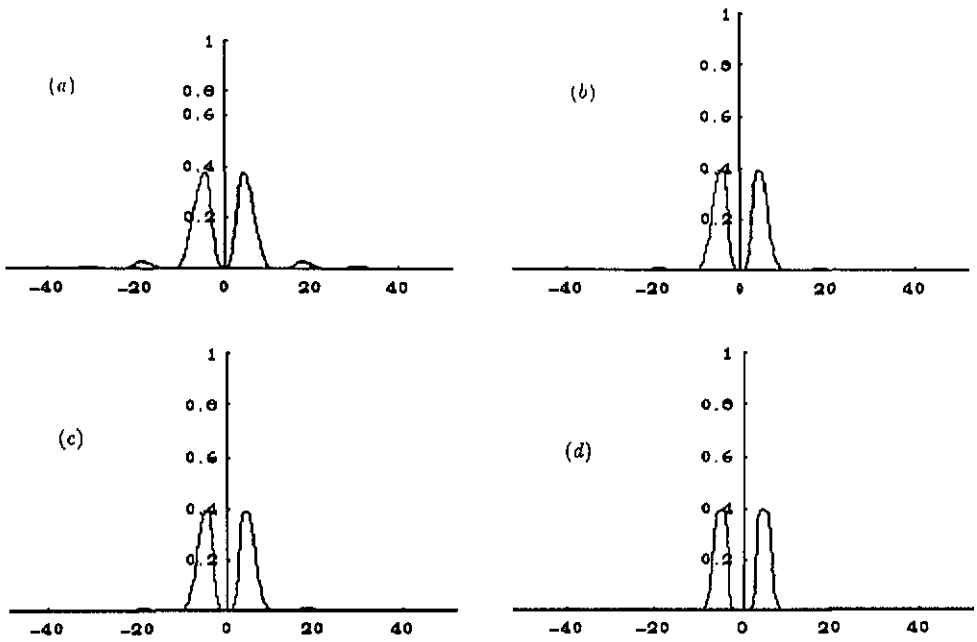

Figure 4. $|\tilde{h}(\omega)|$ for (a) the linear splines, (b) the quadratic splines, (c) the cubic splines, (d) the quartic splines.

$H_{mn}(x, y)$ do not differ too much then a better localization in x necessarily implies a bigger delocalization in y. This feature is well displayed in figure 1. Here we see that the more the wavefunctions are localized in x, the less localized they appear to be in y. The same feature will also be observed in the plots of the other functions.

The Littlewood–Paley basis is, in a certain sense, complementary to the Haar basis. This is related to the fact that it is generated by a mother wavelet which has compact support in the Fourier variable and decays linearly in the configuration space (see (2.1) and (2.2)). Using formula (2.3) [1] we find

$$\Psi^{(\mathrm{LP})}_{mn}(x, y) = \frac{e^{ixy/2}e^{iy2^m n}e^{-(x+2^m n)^2/2}}{\pi^{3/4}}2^{(m-3)/2} \times \left\{\Phi\left(\frac{2\pi - 2^m(y+ix) - in2^{2m}}{2^m\sqrt{2}}\right) - \Phi\left(\frac{\pi - 2^m(y+ix) - in2^{2m}}{2^m\sqrt{2}}\right) + \Phi\left(\frac{2\pi + 2^m(y+ix) + in2^{2m}}{2^m\sqrt{2}}\right) - \Phi\left(\frac{\pi + 2^m(y+ix) + in2^{2m}}{2^m\sqrt{2}}\right)\right\} \tag{3.3}$$

whose asymptotic behaviour, for m and n both zero, has been analysed in [1] and is exactly the opposite of the one obtained for the Haar basis. In general, we can say that the different $\Psi^{(\mathrm{LP})}_{mn}(x, y)$ decay exponentially in y and behave like $1/x$ in x.

In figures $2(a),(b)$ and $3(a),(b)$, we plot the modulus of $\Psi^{(\mathrm{LP})}_{mn}(x, y)$ for $n = 0$ and $m = -6, -3, 0, 3, 6$ for two different ranges of x and y. We see that the delocalization in y increases when m decreases. Apparently, this is in contrast to the remarks we made previously for the Haar basis: in fact, since m now controls the support of $\tilde{h}(\omega)$, it is

possible to repeat analogous steps as before and show that this behaviour can be expected *a priori*. This feature is well displayed by the plots in figures 2(*a*), (*b*) for $m = 3, 0, -3$, while for $m = -6$, the delocalization is so strong that the function $|\Psi^{(LP)}_{-60}(x, y)|$ cannot even be plotted in the figures. This follows from the fact that $|\Psi^{(LP)}_{-60}(x, y)|$ is almost zero in the domain considered. As discussed before, the behaviour of $\Psi^{(LP)}_{m0}(x, y)$ in x, when m varies, is expected to be essentially specular to the behaviour in y in order to keep the normalization of the wavefunctions untouched.

4. The Journé basis

The Journé basis is an example of an orthonormal basis of wavelets of $L^2(\mathbb{R})$ which is not constructed using MRA [7].

It is generated by a mother wavelet, very similar to the one in (2.2),

$$\tilde{\Phi}(\omega) = \begin{cases} (2\pi)^{-1/2} & \text{if } 4\pi/7 \leqslant |\omega| \leqslant \pi \text{ and } 4\pi \leqslant |\omega| \leqslant 32\pi/7 \\ 0 & \text{otherwise} \end{cases} \tag{4.1}$$

which, as we see, has compact support in the Fourier variable and is therefore delocalized in the configuration space. Since $\tilde{\Phi}(\omega)$ is in $L^1(\mathbb{R})$, we can use formula (2.3) to compute the wavefunction in the LLL. The computation is very similar to the one for the Littlewood–Paley basis and gives the following result:

$$\begin{aligned} \Psi^{(J)}_{mn}(x, y) = {} & \frac{e^{ixy/2} e^{iy2^m n} e^{-(x+2^m n)^2/2}}{\pi^{3/4}} 2^{(m-3)/2} \\ & \times \left\{ \Phi\left(\frac{i2^m n - 4\pi 2^{-m} + ix + y}{\sqrt{2}}\right) - \Phi\left(\frac{i2^m n - \pi 2^{-m} + ix + y}{\sqrt{2}}\right) \right. \\ & + \Phi\left(\frac{i2^m n + \pi 2^{-m} + ix + y}{\sqrt{2}}\right) - \Phi\left(\frac{i2^m n + 4\pi 2^{-m} + ix + y}{\sqrt{2}}\right) \\ & - \Phi\left(\frac{i2^m n - \frac{32}{7}\pi 2^{-m} + ix + y}{\sqrt{2}}\right) + \Phi\left(\frac{i2^m n - \frac{4}{7}\pi 2^{-m} + ix + y}{\sqrt{2}}\right) \\ & \left. - \Phi\left(\frac{i2^m n - \frac{4}{7}\pi 2^{-m} + ix + y}{\sqrt{2}}\right) + \Phi\left(\frac{i2^m n + \frac{32}{7}\pi 2^{-m} + ix + y}{\sqrt{2}}\right) \right\}. \end{aligned} \tag{4.2}$$

We see that, apart from a complication arising from the different support of the mother wavelet, the above expression is very similar to the one in (3.3).

The modulus of $\Psi^{(J)}_{mn}(x, y)$ is displayed in figures 3(*a*) and (*b*). As far as the asymptotic behaviour of the above set is concerned, all the considerations discussed about the Littlewood–Paley basis can be repeated: the speed of decay in x is essentially unchanged by the value of m but for the usual normalization considerations. m, however, directly affects the behaviour in y. In particular, we see, from figure 3(*b*), the same feature already observed for the Littlewood–Paley basis. We observe that $\Psi^{(J)}_{-60}(x, y)$ is zero for x, y not too large, while it begins to be different from zero in larger regions (this follows from the increasing delocalization in y when m decreases). We expect that an analogous effect also takes place for $\Psi^{(LP)}_{-60}(x, y)$ even if, in this case, the range we have considered in figures 2(*b*) and (*d*) is still not sufficient to display this delocalization.

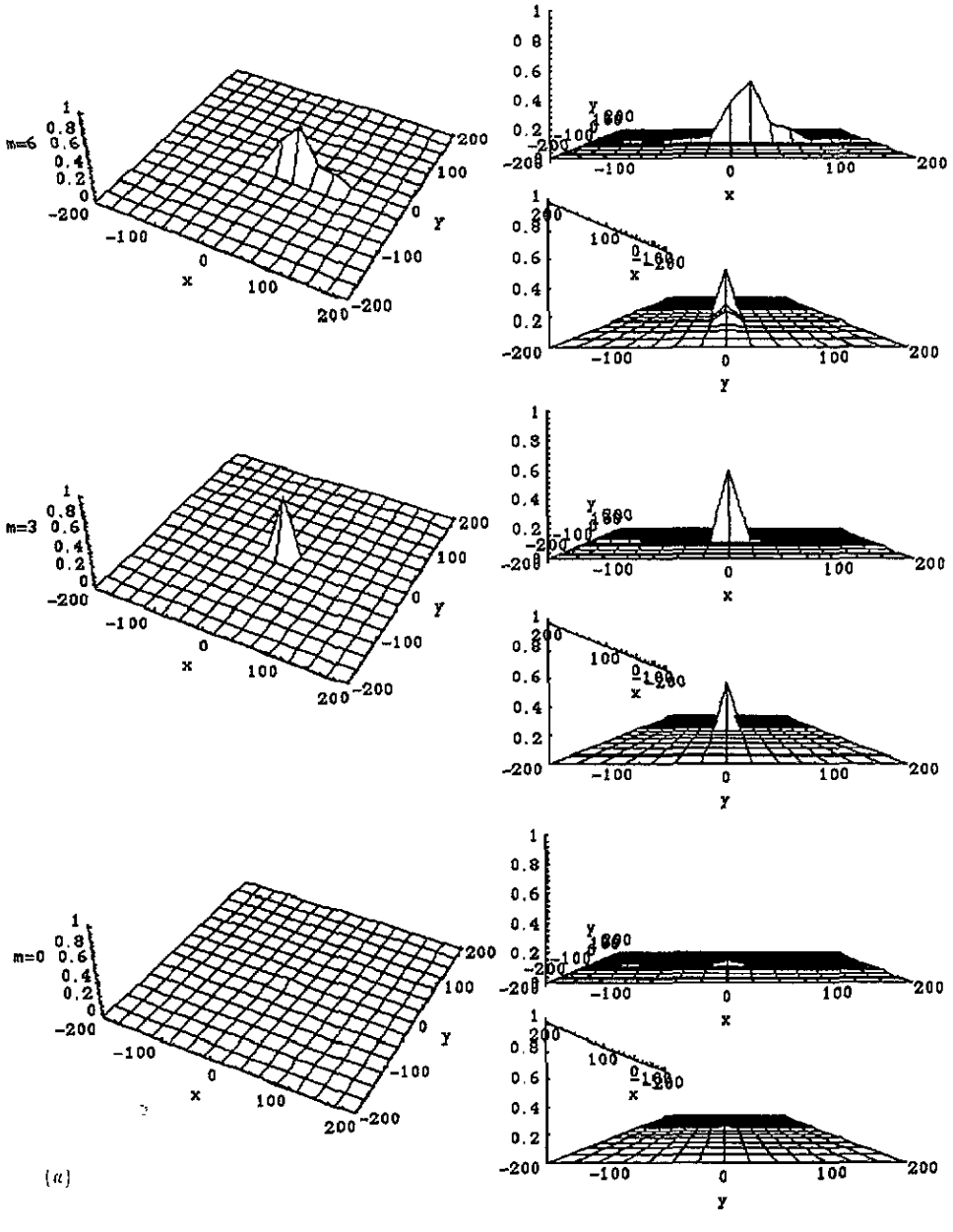

Figure 5. $|\Psi^{(1)}_{m0}(x, y)|$ with (*a*) $m = 6, 3, 0$ and $x, y \in [-200, 200]$; (*b*) $m = -3, -6$ and $x, y \in [-200, 200]$.

5. The spline basis and final remarks

In this section, we discuss the projection in the LLL of some orthonormal spline bases of $L^2(\mathbb{R})$. We discuss, in particular, the linear, quadratic, cubic and quartic splines. The

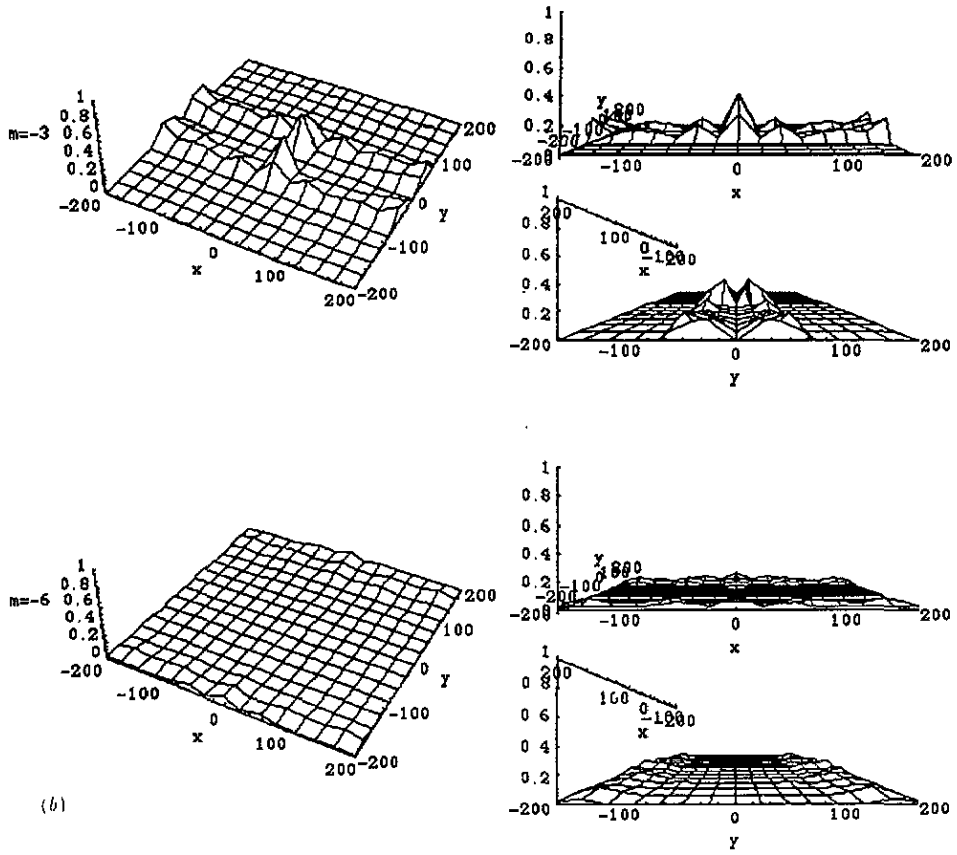

Figure 5. (Continued)

extension of the results to other splines is straightforward.

The essential ingredient for computing the basis is the mother wavelet which originates the orthonormal basis of the LLL via equation (2.3). In [7] it is explained in detail how to build up these functions. The computations are a little tedious and became more difficult as the order of the splines ($N = 1$ for linear splines, $N = 2$ for quadratic splines, and so on) increases. We therefore omit the details and list the mother wavelets in the Fourier variable for $N = 1, 2, 3, 4$:

$$h^{(1)}(\omega) = \sqrt{\frac{3}{2\pi}} e^{i\omega/2} \sin^2(\omega/4) \left(\frac{\sin(\omega/4)}{\omega/4}\right)^2 \sqrt{\frac{2 - \cos(\omega/2)}{(2 + \cos(\omega/2))(2 + \cos(\omega))}} \tag{5.1}$$

$$h^{(2)}(\omega) = \sqrt{\frac{15}{64\pi}} e^{i\omega/4}(3 - e^{-i\omega/2} - 3e^{i\omega/2} + e^{i\omega}) \left(\frac{\sin(\omega/4)}{\omega/4}\right)^3 \times \sqrt{\frac{16 - 13\cos(\omega/2) + \cos(\omega/2)^2}{(16 + 13\cos(\omega/2) + \cos(\omega/2)^2)(16 + 13\cos(\omega) + \cos(\omega)^2)}} \tag{5.2}$$

$$h^{(3)}(\omega) = \sqrt{\frac{315}{16\pi}} e^{i\omega/2}(3 - 4\cos(\omega/2) + \cos(\omega)) \left(\frac{\sin(\omega/4)}{\omega/4}\right)^4 \times \sqrt{\frac{1208 - 1191\cos(\omega/2) + 120\cos(\omega) - \cos(3\omega/2)}{1208 + 1191\cos(\omega/2) + 120\cos(\omega) + \cos(3\omega/2)}} \times \sqrt{\frac{1}{1208 + 1191\cos(\omega) + 120\cos(2\omega) + \cos(3\omega)}} \tag{5.3}$$

$$h^{(4)}(\omega) = \sqrt{\frac{2835}{32\pi}} e^{i\omega/4}(10 - 5e^{-i\omega/2} + e^{-i\omega} - e^{3i\omega/2} + 5e^{i\omega} - 10e^{i\omega/2}) \left(\frac{\sin(\omega/4)}{\omega/4}\right)^5 \times \sqrt{\frac{78\,095 - 88\,234\cos(\omega/2) + 14\,608\cos(\omega) - 502\cos(3\omega/2) + \cos(2\omega)}{78\,095 + 88\,234\cos(\omega/2) + 14\,608\cos(\omega) + 502\cos(3\omega/2) + \cos(2\omega)}} \times \sqrt{\frac{1}{78\,095 + 88\,234\cos(\omega) + 14\,608\cos(2\omega) + 502\cos(3\omega) + \cos(4\omega)}}. \tag{5.4}$$

The moduli of the above functions are plotted in figures 4(*a*)–(*d*). It is interesting to observe that the different functions look very similar to each other and therefore we do not expect big differences in their projection in the LLL. This is, in fact, what we have observed. For this reason we have included in this paper only the figures for the function $\Psi^{(1)}_{mn}(x, y)$.

We start noticing that all the functions $h^{(N)}(\omega)$ belong to $L^1(\mathbb{R})$ due to their behaviour for large ω and, therefore, the equality in formula (2.3) holds true. However, the integration is very hard to perform and no analytic result can be obtained. Nevertheless, it is possible to plot the moduli of the functions using their integral definition directly and this is what we have done to obtain figures 5(*a*) and (*b*). From these figures, it is possible to deduce a lot of information.

We first observe that $\Psi^{(1)}_{30}(x, y)$ appears to be the most localized function in both variables. However, on the contrary, the most delocalized is the function with $m = -6$. A strong delocalization, expecially in x, is also evident for $\Psi^{(1)}_{-30}(x, y)$. It is interesting to note that both $\Psi^{(1)}_{-30}(x, y)$ and $\Psi^{(1)}_{-60}(x, y)$ have an 'unpleasant' behaviour in x and y. They appear to oscillate very much and, from the plots, it is not at all clear how they behave at infinity. Why is this so? It is well known [7] that the spline mother wavelets $h^{(N)}(x)$ ($N = 1, 2, 3, \ldots$) have compact supports in space but each set $\{h^{(N)}_{mn}(x), m, n \in \mathbb{Z}\}$ is made by non-mutually orthogonal functions. In order to obtain orthogonality of the $h^{(N)}_{mn}(x)$ we have to modify the native mother wavelets, losing in this way the original compactness of the supports and obtaining the functions above. Therefore, both the mother wavelet and its Fourier transform have non-compact support; there is no *a priori* reason for having well localized functions in the LLL starting from orthogonal splines.

We end these considerations with a brief comparison between the spline wavefunctions and the other previously introduced functions.

First of all, we notice that the spline wavefunctions seem to be more localized in x than the Journé and the Littlewood–Paley bases for positive m. Due to the oscillations discussed above, the opposite situation holds for negative m. Moreover, they also appear to be less localized in x with respect to the Haar basis. This is expected from the discussion of section 2 since this basis is generated by an x-compactly supported mother wavelet. Similar conclusions could be stated for the behaviour of all these functions in y.

In a future paper we will try to compute the matrix elements of the Coulomb potential in the bases discussed in this paper. Of course, in contrast with what has been done in [2], we will not be able to compute these matrix elements analytically. Nevertheless, it is reasonable to expect that results can be obtained using numerical techniques and these results will be enough to obtain conclusions about the effective utility of MRA and wavelet theory in the search for the true ground state of the FQHE.

This kind of computation has already been performed by the author [9] for a simpler model with many similarities with the FQHE.

In particular, in [9] it is shown that the use of wavelets slightly lowers the trial ground-state energy so that the possibility, discussed in the introduction, of using MRA and wavelets for matching experiments and theory is really at hand.

Acknowledgments

It is a pleasure to thank Dr G Morchio, to whom most of the arguments on asymptotic behaviours in section 2 belong. I also thank Dr R Belledonne for her kind reading of the manuscript.

References

[1] Antoine J P and Bagarello F 1994 *J. Phys. A: Math. Gen.* **27** 2471
[2] Bagarello F, Morchio G and Strocchi F 1993 *Phys. Rev.* B **48** 5306
[3] Laughlin R B 1983 *Phys. Rev.* B **27** 3383
Prangue R E and Girvin S M (ed) 1987 *The Quantum Hall Effect* (New York: Springer)
[4] Khurana A 1990 *Physics Today* (Dec)
Goldman V J, Santos M, Shayegau M and Cunningham J E 1990 *Phys. Rev. Lett.* **65** 2189
[5] Greiter M and McDonald I A 1992 Hierarchy of quantized Hall states in double-layer electron systems *Preprint* IASSNS-HEP 92/64 (Princeton)
[6] Ferrari R 1990 *Phys. Rev.* B **42** 4986
[7] Daubechies I 1992 *Ten Lectures on Wavelets* (Philadelphia: Society for Industrial and Applied Mathematics)
[8] Gradshteyn I S and Ryzhik I M 1980 *Table of Integrals, Series and Products* (New York: Academic)
[9] Bagarello F 1994 *Applications of Wavelets to Quantum Mechanics: a Pedagogical Example* (submitted to ACHA)